# Transform-limited dissipative Kerr solitons with an ultraflat spectrum in a Fabry-Pérot microresonator with a spectral filter

You Yu,[1] Zhiqiang Wang,[2,3,*] Zhen Fang,[1] Yang Li,[1] and Zuxing Zhang[1,†]
[1]*College of Electronic and Optical Engineering & College of Microelectronics, Nanjing University of Posts and Telecommunications, Nanjing 210023, China*
[2]*The Information Materials and Intelligent Sensing Laboratory of Anhui Province, Anhui University, Hefei 230601, China*
[3]*Key Laboratory of Opto-Electronic Information Acquisition and Manipulation of Ministry of Education, Anhui University, Hefei 230601, China*

(Received 17 July 2023; accepted 9 October 2023; published 9 November 2023)

The interplay between the dispersion and spectral filtering effect in Kerr-ring resonators allows the formation of dispersion-less Kerr solitons, an alternative class of Kerr solitons featuring with ultrabroad spectrum and zero chirp. In contrast to a ring resonator, the nonlinear interactions between the counterpropagating light waves in a F-P resonator introduce an additional phase shift, which modifies the system-effective detuning, hence impacting the soliton existence range and its formation dynamics. In this article, we investigate numerically the formation of dissipative Kerr solitons (DKSs) in a 10-mm-long Fabry-Pérot (FP) microresonator with a super-Gaussian spectral filter in the normal dispersion regime. Simulation results found that the spectral loss provided by the filter plays a significant role in the formation of DKS. Without the filter, the FP microresonator yields platicons featuring a flat-top pulse with oscillating tails on both sides. For a super-Gaussian spectral filter with an order of $n \to \infty$, the resonator approaches the transform-limited DKS regime with ultraflat spectrum. An intermediate state of chaotic states of multipulses was observed in the transition from the platicon to the transform-limited DKSs when using the detuning scan technology, the dependence of the appearance of the chaotic state on the spectral filtering effect. Finally, the energy-width scaling behavior and the enhancement of the performances of the transform-limited DKS are studied. Simulation results deepen our understanding of nonlinear dynamics of transform-limited DKS combs and point out a way for achieving a high-energy DKS comb with ultraflat spectrum in Kerr resonators.

DOI: 10.1103/PhysRevA.108.053505

## I. INTRODUCTION

Dissipative Kerr solitons (DKSs) are localized structures that manifest as ultrashort pulses in the time domain and equally spaced coherent spectral lines in the frequency domain [1,2]. In contrast with traditional dissipative solitons in mode-locked lasers [3,4], the formation of DKSs is a result of the balance between the parametric gain and loss in the presence of nonlinearity and dispersion in Kerr resonators [5]. As a new family of optical frequency comb sources [6,7], the realization of DKSs in microresonators has attracted extensive attention in recent years, promoting the development of the chip-scale frequency combs and various practical applications [8,9]. Being basic structures, the DKS has also been widely observed in diverse nonlinear systems [10,11], facilitating the fundamental research on soliton dynamics [12,13].

When referring to DKS, it is bright DKS by default. Besides suffering from the low pump-to-soliton efficiency that is caused by the small overlap between the continuous wave (CW) pump field and the intracavity filed [14], the mandatory requirement of the anomalous dispersion for the formation of the bright DKS in Kerr resonators imposes restrictions on platforms and also limits the DKS performance. For instance, the fabrication of anomalous dispersion microresonators based on $Si_3N_4$ that is complementary metal-oxide semiconductor (CMOS) compatible poses a great challenge to the manufacturing process [15]. Opposite to bright DKSs, the formation of stable structures such as dark pulses [16,17] or platicons [18,19] in normal dispersion Kerr resonators offers an alternative way to improve the pump-to-soliton efficiency [20,21], benefitting the formation of the high-power ultrabroad DKS comb [22].

Stable structures of platicons have been observed in zero-dispersion Kerr resonators in which the third-order dispersion is dominant to balance the nonlinearity instead of the group velocity dispersion (GVD) [23]. In such zero dispersion cavities, the platicon is formed due to the interlocking of two switching waves forming a stable solitary structure with a quantized number of peaks [24]. Interestingly, when the spectral filtering effect involves, a new family of DKS as a result of the balance between nonlinearity and spectral filtering effect has been found in a zero dispersion Kerr-ring resonator. The high-order Gaussian spectral filter with an order of $n \to \infty$ that provides a nearly rectangular transmission function plays a significant role in the formation of the so-called "dispersion-less Kerr solitons" [25]. In comparison to

*zhiqiangwang@ahu.edu.cn
†zxzhang@njupt.edu.cn

 

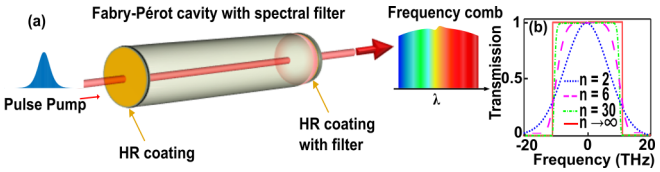


FIG. 1. (a) Schematic diagram of the simulation model of the spectral-filtered normal dispersion FP microresonator pumped by using a sech$^2$ pulse. (b) Spectral transmission of a super-Gaussian filter with different orders.

platicons, the dispersion-less DKS features a single peak pulse without chirp and its spectrum is flat over the entire spectrum with excellent power equilibrium of each comb's teeth, making itself a superior alternative to bright DKS and platicons for applications such as telecommunications [26], light detection and ranging (LIDAR) [27], spectroscopy [28], to mention a few. The mechanism of the formation of the dispersion-less DKS is apparently different from platicons, but the connection and difference between these two different regimes are rarely explored. Also, the formation dynamics of such a type of DKS with ultraflat spectrum in Kerr microresonators also remain elusive and deserve further study, as Kerr microresonators represent a new exciting direction for chip-scale frequency comb generation.

In this article, we numerically investigate the formation dynamics of DKS in a normal dispersion Fabry-Pérot (F-P) microresonator where a super-Gaussian spectral filter is included in the cavity. In contrast to other platforms such as ring Kerr resonators [25], the nonlinear interactions between the counterpropagating light waves in the F-P resonator will introduce an additional phase shift on the intracavity light filed, leading to a change in the system-effective detuning and consequently modifying the soliton formation dynamics. In the spectral-filtered F-P cavity with an order of $n \to \infty$, we observe the formation of stable DKSs with ultraflat spectrum. As without chirp, the formed DKS is termed as transform-limited DKS in the text. The impact of the filter order on the formation of stationary structures in the F-P cavity is studied, revealing the significant role of the spectral filtering effect on the formation of transform-limited DKS. An intermediate state of chaotic multipulses is observed during the transition from the platicon to the transform-limited DKS in the normal dispersion resonator when using detuning scan technology, which distinguishes transform-limited DKSs from platicons. As an additional family of DKS, the energy-scaling behavior of the transform-limited DKS and the optimization of DKS performances are also studied and discussed.

## II. SIMULATION MODEL

The microresonator being studied is a typical F-P resonator [29,30], which is coherently pumped by a pulsed laser source at 1560 nm. A schematic of the numerical model is depicted in Fig. 1(a). The resonator consists of a 10-mm-long highly nonlinear fiber (HNLF) with a high reflective coating of 99.8% at the pump wavelength of 1560 nm on both ends of the fiber. Therefore, the input coupling efficiency of the coherent pump source is only 0.2%. For feasibility, we use pulsed pumping technology to excite the DKS. The pumping pulse is with a sech$^2$ intensity profile and its pulse duration serves as a parameter that varies accordingly for getting the desired DKS state at a certain pumping power. A super-Gaussian spectral filter is introduced in the resonator to perform spectral filtering. Different than the traditional DKS that is a result of the balances between parametric gain and loss in the presence of dispersion and nonlinearity, the order of the super-Gaussian filter serves as the critical parameter for achieving the transform-limited DKS with the ultraflat spectrum in the F-P resonator. Figure 1(b) shows the transmission function of the spectral filter with different orders of $n$, taking the form $T = \exp\{-[2(\omega - \omega_0)/\Delta\omega]^n\}$, where $T$ denotes the transmission function, $\omega_0$ is the central frequency of the filter, $\Delta\omega$ is the filter bandwidth, and $n$ represents the filter order controlling the sharpness of the Gaussian fall-off. When $n = 2$, the filter is a typical Gaussian filter [blue dashed curve in Fig. 1(b)]. With the increase in the order $n$, the filter becomes a super-Gaussian filter with a flat plateau-shaped top and a smooth Gaussian-off [see pink dashed curve and green dashed curve in Fig. 1(b)]. For $n \to \infty$, the transmission of such a filter is close to a gate function with a rectangular shape [red curve in Fig. 1(b)]. The critical role of the spectral filtering effect for achieving transform-limited DKS with ultraflat spectrum in the F-P resonator will be studied later.

Model equations consisting of a nonlinear Schrödinger equation (NSLE) [Eq. (1)] with proper periodic boundary conditions [Eq. (3)] are employed to simulate the nonlinear dynamics in the filter-based normal dispersion F-P Kerr microresonator. An additional phase shift that is dependent on the intracavity average power ($P_{\rm cav}$) is added in the traditional NSLE [31] in the F-P resonator model [see the last term in Eq. (1)]. Being different from Kerr ring resonators, the additional nonlinear integral phase term in the model influences the existence and the formation dynamics of DKS in F-P microresonators [31]

$$\frac{\partial E_m(z,\tau)}{\partial z} = -i\frac{\beta_2}{2}\frac{\partial^2 E_m}{\partial \tau^2} + i\gamma|E_m|^2 E_m + 2i\gamma P_{\rm cav} E_m, \quad (1)$$

$$P_{\rm cav} = \frac{1}{L}\int_0^L |E_m|^2 dz, \quad (2)$$

where $E(z,\tau)$ is the time-varying envelope of the optical field propagating along the $z$ coordinate in resonator. $\beta_2$ is the GVD coefficient and $\gamma$ is the nonlinear coefficient. The subscript $m$ denotes the $m$th roundtrip, $z$ is the propagating distance, and $\tau$ is the retarded time for a pulse moving at the group velocity at the central frequency. The average power $P_{\rm cav}$ can be obtained by integrating the intracavity light field along the resonator. $L$ is the cavity roundtrip length. By solving Eqs. (1) and (2), we can obtain the time domain envelope of the field $E(z = L, \tau)$ after traveling along the HNLF. Then, a filter performs the filtering effect on the field $E(z = L, \omega)$ in the frequency domain before applying the periodic boundary conditions. $E(z = L, \omega)$ is obtained by taking a Fourier transform of the field $E(z = L, \tau)$.

The boundary conditions consider the discrete terms of the pumping field ($P_{in}$), cavity loss ($\alpha$), and the phase detuning ($\delta$) that is defined as the frequency offset between the pumping frequency and the cavity resonance frequency, respectively.

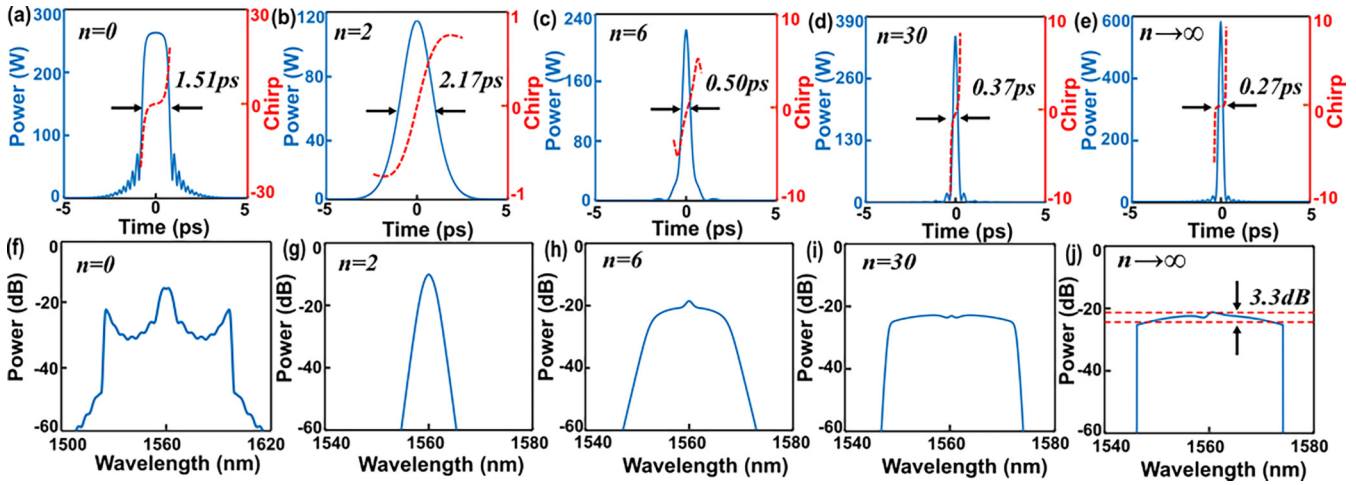


FIG. 2. Simulation results of the pulse intensity profile and the corresponding spectrum in the F-P resonator with a super-Gaussian filter of different orders of $n$. (a)–(e) Pulse intensity profile. The red dash curves are the chirp of pulses. (f)–(j) Spectrum.

Therefore, the input field $E(z=0,\tau)$ at the next roundtrip is given by the expression

$$E_{m+1}(z=0,\tau)=\sqrt{\theta}E_{in}+\sqrt{1-\alpha}e^{-i\delta}E'_m(z=L,\tau), \quad (3)$$

where $\theta$ is the input coupling efficiency of the pump and $\alpha$ is the total cavity roundtrip loss. $E'_m(z=L,\tau)$ is the Fourier transform of the envelope of the intracavity field in the frequency domain after the filter, which is given by

$$E'_m(z=L,\omega)=E_m(z=L,\omega)T$$
$$=E_m(z=L,\omega)\exp\left(-\left[\frac{2(\omega-\omega_0)}{\Delta\omega}\right]^n\right). \quad (4)$$

In the simulations, all the parameters are chosen to match typical experimental values, with $\theta$ of 0.002 and $\alpha$ of 0.006. The fiber parameters are $\beta_2 = 7.5$ ps$^2$/km and $\gamma = 12$ W$^{-1}$/km, respectively. Considering $\beta_2 > 0$ at the pumping wavelength, the resonator operates in the normal dispersion regime. The pulsed pumping field is given by $E_{in} = \sqrt{P_{in}}\,\mathrm{sech}(\tau/\tau_0)$, where $P_{in}$ is the pulse peak power and $\tau_0$ is the temporal duration of the pumping pulse. The initial condition to start the simulation is a weak white noise field, which is generated by using a MATLAB default function. Equation (1) is solved by using the classical split-step Fourier-transform method, where the linear dispersion terms are calculated in the frequency domain and the nonlinear terms are integrated directly in the time domain.

## III. SIMULATION RESULTS

### A. Transform-limited DKS with ultraflat spectrum

We first investigate the DKS formation in F-P microresonators with a superspectral filter. The pumping field is a sech$^2$ pulse characterized by a peak power of 5 W and a pulse duration of 1 ps, respectively. The spectral filter is centered at 1560 nm with a 3-dB bandwidth of 28 nm. We set here the detuning of $\delta = 0.06$ rad. Figure 2 shows the simulation results of the temporal pulse profile and the corresponding spectrum at different filter orders. It is worth noting that, without the filtering effect ($n = 0$), we observe the formation of a typical platicon that features a 1.51-ps flat-top pulse with oscillating tails on both sides of the pulse in the time domain [see in Figs. 2(a) and 2(f)]. Once the filtering effect is involved, for instance, for a typical Gaussian spectral filter with an order of $n = 2$, the intracavity field rapidly converges into a stable DKS characterized by a 2.17-ps Gaussian pulse with a positive chirp. Figures 2(b) and 2(g) show the pulse intensity profile and its corresponding spectrum, respectively. Note that the spectral width of the formed DKS is about 2 nm, far smaller than the spectral filter width. The physical mechanism of the relatively narrow spectrum of the convergent solution of DKS can be attributed to the complicated balances among various physical effects. The spectral filtering shapes the intracavity field in the frequency domain, regulating the strength of SPM. In addition, the parameters including the external coherent pumping and the detuning delicately keep the balance among multiple physical effects. Consequently, stable DKS with a narrow spectrum is achieved.

When a super-Gaussian spectral filter ($n > 2$) with a flat plateau top and smooth Gaussian fall-off is applied, the spectrum of the resultant DKS is confined along with the spectral broadening process. Figure 2(i) demonstrates a rectangle-like spectrum with a 3-dB spectral width of 20 nm at a filter order of $n = 30$, and its corresponding pulse shown in Fig. 2(d) has a pulse duration of 0.37 ps, indicating that the pulse is slightly chirped. The oscillating tails on both sides of the pulse indicate the formation of the ultraflat spectrum. Further increasing the filter order to infinity ($n \to \infty$) leads to a slight broadening of the spectrum until a fully confined spectrum is achieved, which is characterized by its vertical falling edge on both sides of the spectrum. The ultraflat spectrum with the power equilibrium of the comb over the entire spectrum range [see the spectrum in Fig. 2(j)] and the corresponding nearly transform-limited pulse profile [see the pulse intensity profile and its chirp in Fig. 2(e)] demonstrate the uniqueness of the transform-limited DKS, implying its great potential for many practical applications. Note that our simulation results here provide solid evidence for the connection and the distinction between the two intriguing regimes (platicon and transform-limited DKS).

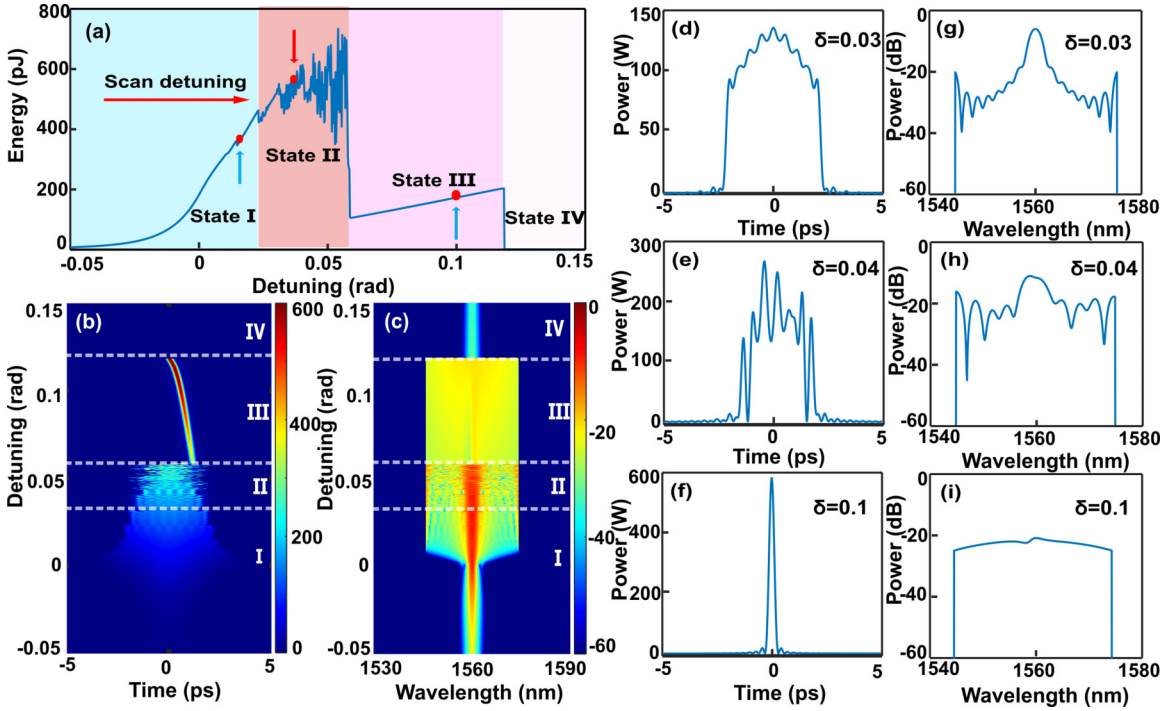


FIG. 3. Formation dynamics of the transform-limited DKS in the F-P microresonator. The peak power of the pumping pulse is 5 W. The filter is a super Gaussian filter with $n \to \infty$ and its spectral bandwidth is 28 nm. (a) Evolution of the intracavity energy in the detuning scan process. (b), (c) Pseudocolor plots of the evolution of the temporal waveforms and spectrum, respectively. (d)–(i) The pulse intensity profile and corresponding spectra at three different detunings.

### B. Formation dynamics of the transform-limited DKS

It is of high interest to investigate how these transform-limited DKSs form in the spectral-filtered normal dispersion F-P microresonator. To this aim, we simulate the evolution of the intracavity field in the F-P resonator at $n \to \infty$ via linearly scanning the detuning $\delta$ from the blue-detuned to the red-detuned region. The pumping field is the same as before (a 1-ps-long sech$^2$ pulse with a peak power of 5 W and the 3-dB spectral width of the filter is 28 nm). As expected, when the detuning crosses the resonance point ($\delta = 0$), stable structures (state I) emerge, followed by a chaotic regime (state II), and then a characteristic soliton step (state III). The evolution process can be reflected by tracing the energy of the intracavity field shown in Fig. 3(a) and also confirmed by the evolution of the intracavity pulse intensity profile [Fig. 3(b)] and of the spectrum [Fig. 3(c)], respectively. This is attributed to the complex dissipative effects of the spectral-correlated loss in the presence of nonlinearity and dispersion in the cavity.

Figures 3(d) to 3(f) show three pulse intensity profiles operating in different regimes at specific detunings, demonstrating the transition from a state of the platicon with multispikes on top [Fig. 3(d)] to a state of a single transform-limited DKS [Fig. 3(f)] through the unstable multi-DKS stage [Fig. 3(e)]. In the entire evolution process, the spectrum is strictly confined by the filter, which is reflected by the intracavity field evolution shown in Fig. 3(c) and the spectra plotted in Figs. 3(g) to 3(i), respectively. As the detuning increases beyond a point where the pump frequency is far from resonance, the decrease in the pump-to-soliton efficiency leads to the disappearance of the DKS state and naturally CW occurs again (state IV). This indicates that the chaotic multi-DKS solutions are an intermediate state between the platicon and transform-limited DKS in Kerr resonators.

### C. Step feature of the transform-limited DKS formation

In prior studies the deterministic formation of the single transform-limited DKS in dispersion-less Kerr resonators is attributed to the direct formation of multi-DKSs with the absence of chaotic solutions during the detuning scan process [25]. In contrast, the scenario of the occurrence of chaotic multipulse solutions that we observe in the evolution of the intracavity field via detuning scan in the normal dispersion regime suggests that the chaotic regime is not an essential approach for the system developing transform-limited DKS. Hence, it is interesting to investigate the soliton step feature of the transform-limited DKS formation under different pump conditions. Here, we take a 4 ps-long pulse with a peak power of 5 W as the pumping pulse and study the evolution of the intracavity field in the F-P microresonator at a filter order of $n = 30$. The 3-dB width of the filter remains 28 nm. Figure 4(a) depicts the pulse energy evolution of the intracavity field. In this case, the energy trace of the intracavity field during the detuning scan shows clearly soliton transition steps, suggesting the formation of multi-DKSs (also called "soliton molecules") when the detuning crosses the resonance. Further scanning the detuning towards the red-detuned region leads to the annihilation of pulses in the multi-DKS state one by one until a single transform-limited DKS is formed in the end. We note the absence of some intermediate states in the soliton leap step (for instance, 3 DKSs and 2 DKSs), which can be attributed to the narrow soliton existence range that can be

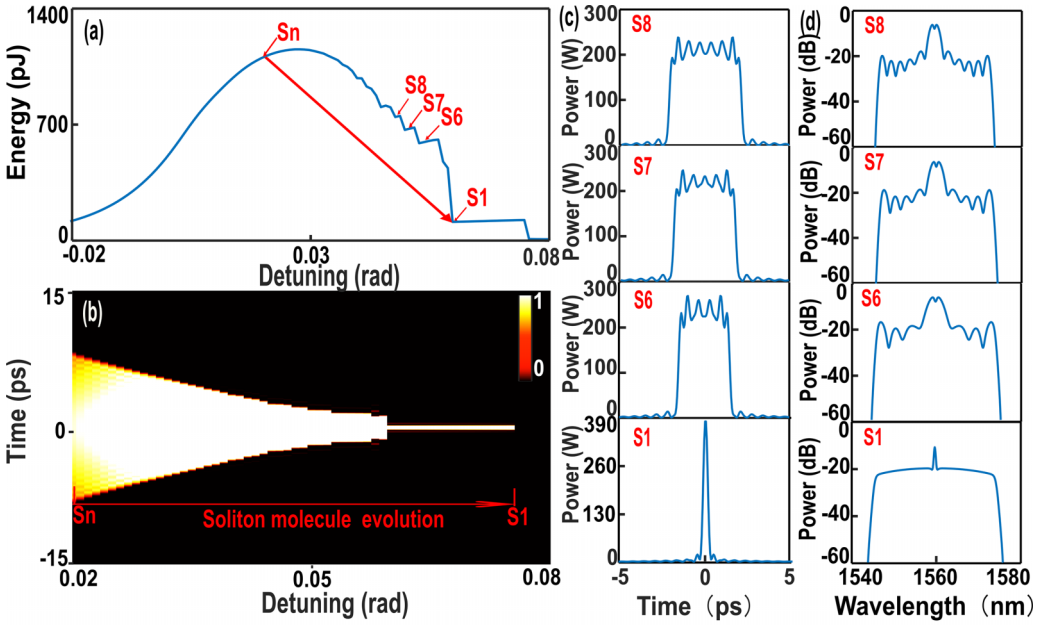


FIG. 4. Evolution dynamics of deterministic generation of single transform-limited DKS in a normal dispersion F-P microresonator with a super-Gaussian filter of $n = 30$. The pumping pulse peak power is 5 W. The filter spectral width is 28 nm. S8, S7, S6, and S1 denote the number of pulses contained in the soliton molecule structures. (a) Evolution of the intracavity energy and (b) Temporal intensity profile evolution in the detuning scan process. (c), (d) Time domain profiles and spectra for four different states.

observed. Figures 4(c) and 4(d) present four typical states of the pulse intensity profile and the corresponding spectrum in the DKS annihilation process, respectively. The multispikes on the top of the pulse intensity profile are a signature of the number of solitons in the states, and the modulation on the top of the well-confined spectrum is because of the interference among pulses. Interestingly, there are no chaotic solutions appearing in this case. The comparison of the evolving dynamics shown in Figs. 3 and 4 reveals the dependence of the occurrence of the chaotic multipulse state on the spectral filtering effect. The slight change in the pumping condition pushes the laser system to go through different paths toward the deterministic state of the single transform-limited DKS in the resonator.

### D. Energy-width scaling behavior of the transform-limited DKS

In this section, we study the energy-width scaling behavior of the transform-limited DKS in the proposed F-P microresonator. As the spectrum of the transform-limited DKS is well confined by the spectral filter, its energy-width scaling behavior is expected to be different than traditional optical solitons whose energy and pulse duration obey the condition of $E_P = 2|\beta_2|/(\gamma\tau)$, where $E_P$ is the pulse energy and $\tau$ is the pulse duration. Figure 5(a) shows the existence map of different nonlinear solutions in the filter-based F-P microresonator in a two-dimensional parameter space in the plane of $(\delta, P_{in})$ by solving the Ikeda map of the system at different pumping power. The pumping pulse is a $\mathrm{sech}^2$ pulse with a pulse duration of 1 ps and the spectral filter is a high-order Gaussian filter with $n \to \infty$. The color represents the intracavity energy, hence different colors indicate regions for different nonlinear solutions. First, we see the appearance of different nonlinear solutions and the transition among them during the detuning scan process. The white dashed lines show clear boundaries of different solutions. State I corresponds to the pattern of the modulation stabilities (MI) that are caused by the periodic spectral loss of the filter, state II stands for chaotic multipulses, state III represents the single transform-limited DKS state, and state IV is for the CW operation. Second, we observe an expansion of the existence range for the transform-limited DKS as the pumping power increases, which is a typical behavior commonly observed in diverse Kerr resonator systems.

The point of this section is to study the energy-width scaling behavior of the transform-limited DKS. To this end, we plot in Figs. 5(b) to 5(d) the pulse energy and duration of DKS solutions [labeled as red stars in Fig. 5(a)] as a function of the detuning at a fixed pumping power of 5 W. Although the pulse energy does increase linearly as the detuning increases [blue curve in Fig. 5(b)], the pulse duration of DKS remains constant [red star curve in Fig. 5(b)], besides the growth of the pulse peak power and its intensity profile. The invariable 3-dB spectral width shown in Fig. 5(d) also provides a signature of the constant pulse duration. The self-similarly evolving pulse and its spectrum distinguish the transform-limited DKS from traditional DKSs. At a constant of the detuning of $\delta = 0.1$ rad, when the pumping power is increasing, the evolution of the pulse parameters of the transform-limited DKS exhibits similar dynamics. The pulse duration remains unchanged while the pulse energy increases linearly as the pumping power increases. The unique energy-width scaling behavior of the transform-limited DKS makes itself an alternative for realizing high-energy DKS comb in Kerr resonators.

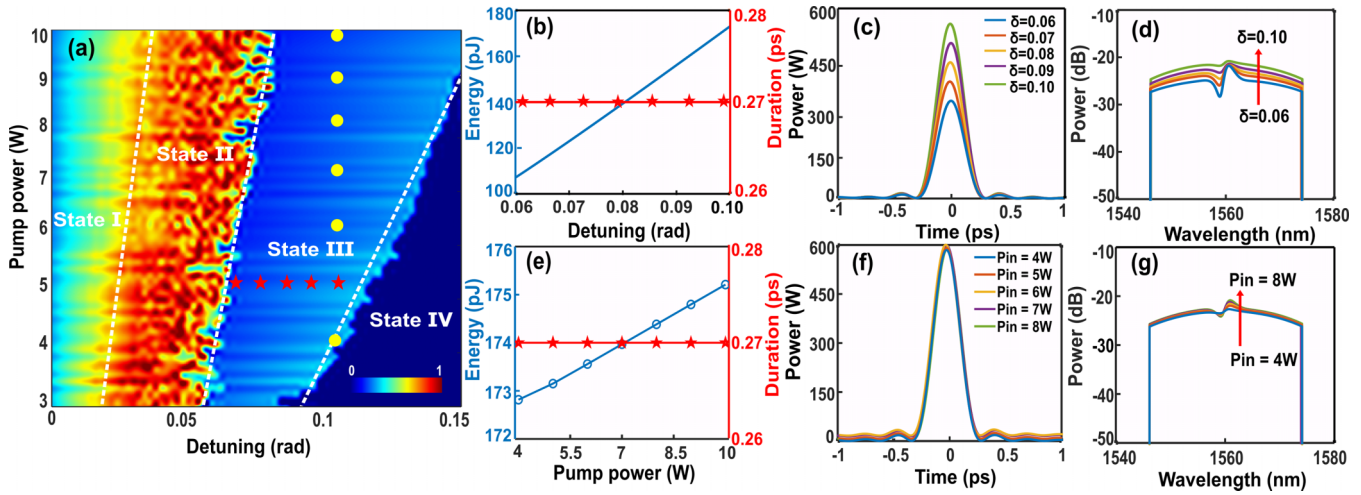


FIG. 5. (a) Existence range of different solutions in the two-dimensional parameter space in the plane of $(P_{in}, \delta)$. State I: Region of the parameter space for modulation instability (MI). State II: The chaotic patterns. State III: Transform-limited DKS. State IV: CW region. (b) Evolution of pulse energy (left) and duration (right) as a function of detuning at a fixed pumping power of 5 W. (c) Pulse profiles at different detuning and (d) the corresponding spectrum profile. (e) Pulse energy (left) and its duration (right) as a function of pump power at a constant detuning of $\delta = 0.1$ rad. (f) Pulse profile at different pumping power and (g) the corresponding spectra.

### E. Effect of the filter width on the performance of the transform-limited DKS

Concerning the features of the zero chirp and ultraflat spectrum of the transform-limited DKS that is attracted for practical applications, it is worth studying the optimization of the DKS performances in the F-P microresonator. The peak power of the pulsed pumping field is 5 W and the pulse duration of 1 ps. The dependence of the DKS performances on the filter width ($\Delta\lambda$) is studied. By scanning the detuning for five different filter widths, we observe clearly the soliton steps from the evolution of the intracavity energy trace [see in Fig. 6(a)], demonstrating an inverse relation between the pulse energy and $\Delta\lambda$. Figures 6(c) and 6(d) present the pulse intensity profile and the corresponding spectrum for different $\Delta\lambda$ at the detuning of $\delta = 0.1$ rad. For a relatively small $\Delta\lambda$, the resonator yields the transform-limited DKS with a relatively wider pulse duration and higher pulse energy but with a narrower spectrum that is confined by the filter width. As shown in Fig. 6(b), the larger the value of $\Delta\lambda$, the narrower the pulse is, and naturally the broader the spectrum is. Also, the spectrum of the DKS for a wider spectral filter becomes flatter, which is an attractive feature for practical applications. In contrast to the energy-width scaling law for traditional solitons, the transform-limited DKS behaves differently. The widest spectrum width we obtain in simulations is 36 nm and its corresponding pulse duration is about 270 fs. Further optimization of the performance of the transform-limited DKS can be obtained by increasing the pumping power and using a wider spectral filter.

## IV. CONCLUSION

In conclusion, we numerically studied the formation of the transform-limited DKS in a normal dispersion F-P microresonator with a spectral filter. Via scanning the detuning from the blue-detuned to the red-detuned region, a single transform-limited DKS is deterministically formed through a transition process in which a bound state of multipulses are initially formed at certain detuning point and then annihilated one by one along with the detuning scans until only one survives. Before the onset of DKS operation, we observed an intermediate state of chaotic multipulses during the transition from the platicon to the transform-limited DKS state, which distinguished the transform-limited DKS from platicon. Due to the composite balance between the spectral loss and parametric gain in the presence of dispersion and nonlinearity,

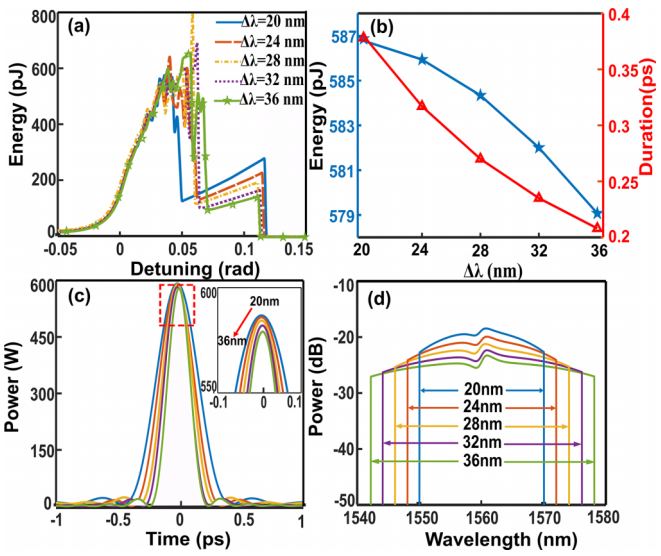


FIG. 6. The dependence of the performances of the transform-limited DKS for five different spectral widths. The pumping pulse peak power is 5-W pump power. (a) Evolution of the intracavity energy as the detuning scans. (b) The pulse energy (cyan curves) and pulse duration (red curves) as a function of the spectral filter width. (c) Time profile of the transform-limited DKS and (d) spectrum profile for five different filter bandwidths at a detuning of $\delta = 0.1$ rad.

the DKS had nearly zero chirp and an ultraflat spectrum. The energy-width scaling behavior of the transform-limited DKS was also studied, revealing the constant pulse duration and the self-similarly evolving in the spectrum and pulse profile in the process of increasing the pumping power. By optimizing the filter width, an ultrashort of 270 fs DKS with nearly zero chirp was obtained at a spectral filter width of 36 nm and a detuning of $\delta = 0.1$ rad. Further enhancement in the performances of the transform-limited DKS is possible by optimizing the pumping field and the spectral filter parameters. Simulation results hence provide an alternative way to obtain the high-energy dissipative soliton comb in Kerr resonators, which has great potential for applications in the fields of telecommunications, spectroscopy, and precision measurement, to mention a few.

In addition to the additional nonlinear phase shift term introduced by the F-P configuration, spectral filters with different spectral response functions also impact the effective detuning of the system due to its frequency-dependent transmission. One consequence of the spectral filtering is the effect on the existence range of DKS, and a second consequence is the impact on the evolution and formation of nonlinear solutions in the systems. For instance, at a filter order of $n = 30$, no solution of chaotic states was observed when using the detuning scan technology to excite DKS. However, for a case of $n \to \infty$, an intermediate chaotic state of multipulses was observed in the transition from platicon to the DKS state. Further detailed investigation of the formation of DKS in the F-P cavity containing different types of filters may reveal interesting differences, which is out of the scope of our present work.

Finally, we would like to stress that our work demonstrates the formation of transform-limited DKS in a spectral-filtered normal dispersion F-P resonator, rather than ring resonators [25]. An additional nonlinear phase term should be considered when using the Lugiato-Lefever equation (LLE) or nonlinear Schrödinger equation (NLSE) with proper boundary conditions to describe the system behavior. Therefore, our simulation results provide guidance for the experimental realization of such a type of DKS in other compact, on-chip integrated microresonator platforms. Although it may be challenging to experimentally coat super-Gaussian spectral filters with ideal transmission and neglectable losses on F-P cavities as we implemented in simulations, the realization of stable DKS in low-$Q$-factor cavities may ease the requirement of the low-loss spectral filter for the realization of transform-limited DKS in the spectral-filtered F-P resonators [32].

## ACKNOWLEDGMENTS

This work was supported by the National Natural Science Foundation of China under Grant No. 62375001, the Talent start-up fund of Anhui University Grant No. S020318030/009 and partially supported by National Natural Science Foundation of China under Grant No. 62175116; Key R&D Plan of Jiangxi Province Grants No. 20212BBE51005 and No. 1311 talent plan of Nanjing University of Posts and Telecommunications.

[1] F. Leo, S. Coen, P. Kockaert, S.-P. Gorza, P. Emplit, and M. Haelterman, Temporal cavity solitons in one-dimensional kerr media as bits in an all-optical buffer, Nat. Photon. **4**, 471 (2010).

[2] T. J. Kippenberg, R. Holzwarth, and S. A. Diddams, Microresonator-based optical frequency combs, Science **332**, 555 (2011).

[3] P. Grelu and N. Akhmediev, Dissipative solitons for mode-locked lasers, Nat. Photon. **6**, 84 (2012).

[4] B. G. Bale, S. Boscolo, and S. K. Turitsyn, Dissipative dispersion-managed solitons in mode-locked lasers, Opt. Lett. **34**, 3286 (2009).

[5] T. J. Kippenberg, A. L. Gaeta, M. Lipson, and M. L. Gorodetsky, Dissipative kerr solitons in optical microresonators, Science **361**, eaan8083 (2018).

[6] P. Del'Haye, A. Schliesser, O. Arcizet, T. Wilken, R. Holzwarth, and T. J. Kippenberg, Optical frequency comb generation from a monolithic microresonator, Nature (London) **450**, 1214 (2007).

[7] T. Herr, V. Brasch, J. D. Jost, C. Y. Wang, N. M. Kondratiev, M. L. Gorodetsky, and T. J. Kippenberg, Temporal solitons in optical microresonators, Nat. Photon. **8**, 145 (2014).

[8] M.-G. Suh and K. J. Vahala, Soliton microcomb range measurement, Science **359**, 884 (2018).

[9] D. T. Spencer *et al.*, An optical-frequency synthesizer using integrated photonics, Nature (London) **557**, 81 (2018).

[10] H. Zhou, Y. Geng, W. Cui, S.-W. Huang, Q. Zhou, K. Qiu, and C. Wei Wong, Soliton bursts and deterministic dissipative kerr soliton generation in auxiliary-assisted microcavities, Light Sci. Appl. **8**, 50 (2019).

[11] F. Yang, Z. Wang, and Z. Zhang, Generation of dissipative kerr solitons in a passive fiber kerr resonator with a fast saturable absorber, Phys. Rev. A **107**, 013530 (2023).

[12] C. Godey, I. V. Balakireva, A. Coillet, and Y. K. Chembo, Stability analysis of the spatiotemporal lugiato-lefever model for kerr optical frequency combs in the anomalous and normal dispersion regimes, Phys. Rev. A **89**, 063814 (2014).

[13] T. Herr, K. Hartinger, J. Riemensberger, C. Wang, E. Gavartin, R. Holzwarth, M. Gorodetsky, and T. Kippenberg, Universal formation dynamics and noise of kerr-frequency combs in microresonators, Nat. Photon. **6**, 480 (2012).

[14] X. Xue, P.-H. Wang, Y. Xuan, M. Qi, and A. M. Weiner, Microresonator kerr frequency combs with high conversion efficiency, Laser Photon. Rev. **11**, 1600276 (2017).

[15] Y. Xie, J. Li, Y. Zhang, Z. Wu, S. Zeng, S. Lin, Z. Wu, W. Zhou, Y. Chen, and S. Yu, Soliton frequency comb generation in cmos-compatible silicon nitride microresonators, Photon. Res. **10**, 1290 (2022).

[16] X. Xue, Y. Xuan, Y. Liu, P.-H. Wang, S. Chen, J. Wang, D. E. Leaird, M. Qi, and A. M. Weiner, Mode-locked dark pulse kerr combs in normal-dispersion microresonators, Nat. Photon. **9**, 594 (2015).

[17] E. Nazemosadat, A. Fülöp, Ó. B. Helgason, P.-H. Wang, Y. Xuan, D. E. Leaird, M. Qi, E. Silvestre, A. M. Weiner *et al.*, Switching dynamics of dark-pulse kerr frequency comb states in optical microresonators, Phys. Rev. A **103**, 013513 (2021).

[18] V. Lobanov, G. Lihachev, T. Kippenberg, and M. Gorodetsky, Frequency combs and platicons in optical microresonators with normal gvd, Opt. Express **23**, 7713 (2015).

[19] G. Lihachev, W. Weng, J. Liu, L. Chang, J. Guo, J. He, R. N. Wang, M. H. Anderson, Y. Liu, J. E. Bowers *et al.*, Platicon microcomb generation using laser self-injection locking, Nat. Commun. **13**, 1771 (2022).

[20] B. Y. Kim, Y. Okawachi, J. K. Jang, M. Yu, X. Ji, Y. Zhao, C. Joshi, M. Lipson, and A. L. Gaeta, Turn-key, high-efficiency kerr comb source, Opt. Lett. **44**, 4475 (2019).

[21] X. Xue, X. Zheng, and B. Zhou, Super-efficient temporal solitons in mutually coupled optical cavities, Nat. Photon. **13**, 616 (2019).

[22] C. Spiess, Q. Yang, X. Dong, V. G. Bucklew, and W. H. Renninger, Chirped dissipative solitons in driven optical resonators, Optica **8**, 861 (2021).

[23] M. H. Anderson, W. Weng, G. Lihachev, A. Tikan, J. Liu, and T. J. Kippenberg, Zero dispersion kerr solitons in optical microresonators, Nat. Commun. **13**, 4764 (2022).

[24] P. Parra-Rivas, D. Gomila, and L. Gelens, Coexistence of stable dark-and bright-soliton kerr combs in normal-dispersion resonators, Phys. Rev. A **95**, 053863 (2017).

[25] X. Xue, P. Grelu, B. Yang, M. Wang, S. Li, X. Zheng, and B. Zhou, Dispersion-less kerr solitons in spectrally confined optical cavities, Light Sci. Appl. **12**, 19 (2023).

[26] P. Marin-Palomo, J. N. Kemal, M. Karpov, A. Kordts, J. Pfeifle, M. H. Pfeiffer, P. Trocha, S. Wolf, V. Brasch, M. H. Anderson *et al.*, Microresonator-based solitons for massively parallel coherent optical communications, Nature (London) **546**, 274 (2017).

[27] J. Riemensberger, A. Lukashchuk, M. Karpov, W. Weng, E. Lucas, J. Liu, and T. J. Kippenberg, Massively parallel coherent laser ranging using a soliton microcomb, Nature (London) **581**, 164 (2020).

[28] M.-G. Suh, Q.-F. Yang, K. Y. Yang, X. Yi, and K. J. Vahala, Microresonator soliton dual-comb spectroscopy, Science **354**, 600 (2016).

[29] E. Obrzud, S. Lecomte, and T. Herr, Temporal solitons in microresonators driven by optical pulses, Nat. Photon. **11**, 600 (2017).

[30] Z. Xiao, K. Wu, T. Li, and J. Chen, Deterministic single-soliton generation in a graphene-fp microresonator, Opt. Express **28**, 14933 (2020).

[31] D. C. Cole, A. Gatti, S. B. Papp, F. Prati, and L. Lugiato, Theory of kerr frequency combs in fabry-perot resonators, Phys. Rev. A **98**, 013831 (2018).

[32] X. Dong, C. Spiess, V. G. Bucklew, and W. H. Renninger, Chirped-pulsed kerr solitons in the lugiato-lefever equation with spectral filtering, Phys. Rev. Res. **3**, 033252 (2021).